Journal of Theoretical and Applied Vibration and Acoustics 1(2) 62-72 (2015)

I S A V

Journal of Theoretical and Applied Vibration and Acoustics

journal homepage: http://tava.isav.ir

Transverse vibration and instability of fluid conveying triple-walled carbon nanotubes based on strain-inertia gradient theory

Soheil Oveissi [a], **Hassan Nahvi** [b*]

[a] *Department of Mechanical Engineering, Islamic Azad University, Khomeinishahr Branch, 84175/119, Khomeinishahr, Isfahan, Iran*

[b] *Department of Mechanical Engineering, Isfahan University of Technology, Isfahan 8415683111, Iran*

KEYWORDS

Triple-walled carbon nanotube

Knudsen number

Strain-inertia gradient theory

Galerkin's method

ABSTRACT

In this paper, the transverse vibration of a triple-walled carbon nanotube (TWCNT) conveying fluid flow is studied based on the strain/inertia gradient theory with van der Waals interaction taken into consideration. The nanotube is modelled using Euler-Bernoulli beam model and the Galerkin's method is employed to obtain the CNT complex valued Eigen-frequencies. The effects of the fluid flow thorough the innermost tube and the van der Waals force interaction between any two walls on the instability of the nanotube are studied. In addition, the effects of the nano-flow size, the characteristic lengths and the aspect ratio on the critical flow velocities are investigated. Results indicate that due to the fluid flow the nanotube natural frequencies decrease. By considering the size effect of the fluid flow, frequencies decrease more rapidly causing reduction of the stability region. Moreover, it is shown that the length of the nanotube can play an important role in the vibration response.

1. Introduction

Carbon nanotubes with their excellent properties have applications in fields such as nanotubes conveying fluid [1], nano fluidic devices [2], drug delivery devices [3], micromechanical oscillators, sensors, etc. [4]. To this end, many researchers focused on the interesting dynamic characteristics of fluid-structure systems in small-scale [5, 6]. Due to the fact that molecular dyn0amics simulations (MDS) are complex and time consuming, using the classical continuum mechanics theories can be an effective and useful way to study mechanical behaviour of both single-walled and multi-walled carbon nanotubes. Rafiei et al. [7] discussed the effects of taper ratio and small-scale parameter on the vibration of non-uniform carbon nanotubes. They reported that dimensionless frequencies obtained from nonlocal theory are less than those obtained from local ones. Wang [8] utilized nonlocal elasticity theory integrated with surface elasticity theory to model the fluid conveying nanotubes with inner and outer surface layers. He showed that the

* Corresponding Author: Hassan Nahvi, Email: hasnahvi@yahoo.com

predicted fundamental frequency is generally higher than that predicted by the Euler-Bernoulli beam model without surface effects. Yoon et al. [9] investigated transverse sound wave propagation in multi-walled carbon nanotubes (MWCNTs) based on the multiple-elastic beam model. Yan et al. [10] studied the dynamical characteristics of the fluid-conveying MWCNTs by using the classical continuum theory. They reported that the van der Waals (vdW) interaction has no influence on the bifurcation of the system. Rashidi et al. [11] presented a model for a single mode coupled vibration of fluid conveying CNTs considering the slip boundary conditions of nano flow. They found that the critical flow velocities decrease if the passage fluid is a gas with nonzero Kn in contrast to a liquid nano flow.

In this research, the effect of small size for both fluid flow and solid structure is considered on the of vibration study of CNT. Also, for the first time, by using the Euler-Bernoulli beam theory a model is proposed for the coupled vibrations of triple-walled carbon nanotubes conveying fluid flow taking into account the small-size effects of both flow fluid and solid structure utilizing Knudsen number and strain-inertia gradient theory. In addition, the influences of small-size effects and aspect ratio on the natural frequencies are investigated. For the numerical solution, the governing fluid-structure equation is discretized by using the Galerkin method. It has been shown that the size-effect has significant influence on the non-dimensional critical flow velocities. Moreover, it is found that the length and CNT radius have effect on the natural frequencies and critical flow velocities.

2. Strain-inertia gradient theory

The theory of combined strain-inertia gradient is developed by Askes and Aifantis [12]. They showed that the combination of equation of motion and the strain-inertia gradient constitutive relation can be expressed as

$$\rho(\ddot{u}_i - l_m^2 \ddot{u}_{i,mm}) = C_{ijkl}(u_{k,jl} - l_s^2 u_{k,jlmm}) \tag{1}$$

where ρ is the mass density of nanostructure, C_{ijkl} are Cartesian components of elasticity tensor and u_i denotes the Cartesian displacements for an elastic structure. Also l_m and l_s are the two length scales related to the inertia and strain gradients respectively, which represent volume element sizes of electrostatics and electrodynamics problems.

According to this theory, the CNT conveying fluid remains more stable compared to the classical theories [13]. Setting $i = 3$ and using the linearized strain-displacement relation of the Euler-Bernoulli beam theory yields the constitutive relation for 1-D Euler-Bernoulli beam model.

The bending moment is

$$M = \int_A z\sigma dA \tag{2}$$

where σ denotes the flexural or axial stress. According to the strain-inertia gradient theory, the stress-strain relation may be written as

$$\sigma = \sigma_{xx} = E\left(\varepsilon - l_s^2 \frac{\partial^2 \varepsilon}{\partial x^2}\right) + \rho_c l_m^2 \frac{\partial^2 \varepsilon}{\partial t^2} \tag{3}$$

in which ε is the bending strain that for 1-D strain-flexural curvature can be written as,

$$\varepsilon = \varepsilon_{xx} = -z\left(\frac{\partial^2 w}{\partial x^2}\right) \tag{4}$$

Finally, by integrating over the beam cross-sectional area, Eq. (2) gives;

$$M = -EI\left(\frac{\partial^2 w}{\partial x^2} - l_s^2 \frac{\partial^4 w}{\partial x^4}\right) - \rho_c I l_m^2 \frac{\partial^4 w}{\partial x^2 \partial t^2} \tag{5}$$

3. Size effect of nano flow

To investigate the small-scale effect of nano flow, the velocity correction factor (VCF) is inserted into the fluid-structure interaction equation of motion multiplied by the flow velocity term. By considering the VCF parameter, the fluid slip-boundary condition can be inserted into the equation of motion. VCF parameter is defined as follows [11].

$$VCF = \frac{V_{slip}}{V_{(no-slip)}} = \frac{1}{Cr(kn)}\left(4\left(\frac{2-\sigma_v}{\sigma_v}\right)\left(\frac{Kn}{1-bKn}\right)+1\right) \tag{6}$$

where V_{slip} and $V_{(no-slip)}$ are the flow velocities with and without slip boundary conditions respectively. Also σ_v and b are the tangential momentum accommodation coefficient and the general slip coefficient; these two parameters are considered to be 0.7 and -1 respectively. Parameter Cr is the rarefaction coefficient which is defined as follows by using the Polard relation for viscous fluids [14].

$$Cr(Kn) = \frac{1}{1+\alpha Kn} \tag{7}$$

where α is a constant obtained as,

$$\alpha = \frac{2}{\pi}\alpha_0[\tan^{-1}(\alpha_1 Kn^B)] \tag{8}$$

in which $\alpha_0 = 64/3\pi(1-(4/b))$, $\alpha_1 = 0.4$ and $B = 0.4$ are practical parameters. In Eq. (6), the effective parameter is Knudsen number (Kn) that presents the ratio of the free path of the fluid molecules to a characteristic length of the flow geometry. The range of Kn can vary from 0.001 to 0.01 for a liquid nano flow [11].The values of the parameters in Eqs. (6)-(8) are extracted from [12].

4. Governing equations

Flexural vibration of the Euler-Bernoulli beam model is studied using the equations of motion of the CNTs. The external force can be considered as an incompressible, laminar, infinite and viscous fluid flowing through the CNT. On the other hand, the TWCNTs consist of three single SWCNTs with the van der Waals interaction between any two tubes, as shown in Fig. 1(a). The fluid flows inside the innermost tube of the CNT. Based on the strain-inertia gradient theory, the

innovative governing 1-D coupled fluid-structure interaction equations of motion for a TWCNT conveying fluid are derived as

(9)

$$EI_1\left(\frac{\partial^4 W_1}{\partial x^4}-l_s^2\frac{\partial^6 W_1}{\partial x^6}\right)+(m_{c_1}+m_f)\frac{\partial^2 W_1}{\partial t^2}+m_f(VCF)^2U^2\frac{\partial^2 W_1}{\partial x^2}+2m_f(VCF)U\frac{\partial^2 W_1}{\partial t\partial x}+\rho_c I l_m^2\frac{\partial^6 W_1}{\partial t^2\partial x^4}=f_1$$

$$EI_2\left(\frac{\partial^4 W_2}{\partial x^4}-l_s^2\frac{\partial^6 W_2}{\partial x^6}\right)+m_{c_2}\frac{\partial^2 W_2}{\partial t^2}=f_2$$

$$EI_3\left(\frac{\partial^4 W_3}{\partial x^4}-l_s^2\frac{\partial^6 W_3}{\partial x^6}\right)+m_{c_3}\frac{\partial^2 W_3}{\partial t^2}=f_3$$

where W_1, W_2 and W_3 denote the flexural displacements of the innermost, middle and outermost CNT walls respectively. Also x is the axial coordinate, E is the beam's Young modulus and U is the flow velocity. In addition, I_1, I_2 and I_3 are the moments of inertia related to the three walls of CNT and m_f is the fluid mass per unit length. Parameters m_{c_1}, m_{c_2} and m_{c_3} are the mass per unit length of inner, middle and outer CNTs respectively.

In Eq. (9), f_1, f_2 and f_3 denote the acting Van der waals interaction forces exerted on the inner, middle and outer CNT walls due to the van der Waals interaction among any two walls. These forces can be expressed as,

$$f_i(x,0)=\sum_{j=1,i\neq j}^{3}c_{ij}(W_i-W_j) \tag{10}$$

for $i=1,2,3$ where c_{ij} is the van der Waals coefficient for the related CNT wall that can be obtained as [10],

$$c_{ij}=-R_i\left[\frac{1001\pi\varepsilon\sigma^{12}}{3a^4}E_{ij}^{13}-\frac{1120\pi\varepsilon\sigma^{6}}{9a^4}E_{ij}^{7}\right]R_j \tag{11}$$

in which

$$E_{ij}^{n}=(R_i+R_j)^{-n}\int_0^{\pi/2}\frac{d\theta}{[1-K_{ij}\cos^2\theta]^{l/2}} \tag{12}$$

$$K_{ij}=\frac{4R_jR_i}{(R_j+R_i)^2} \tag{13}$$

The equation of motion may be rendered dimensionless. For this purpose, the following dimensionless variables are defined

$$\xi=\frac{x}{L},\quad \eta_1=\frac{W_1}{L},\quad \eta_2=\frac{W_2}{L},\quad \eta_3=\frac{W_3}{L},\quad \tau=\left[\frac{EI_1}{m_f+m_{c_1}}\right]^{\frac{1}{2}}\frac{t}{L^2},\quad u_n=\left(\frac{m_f}{EI_1}\right)^{\frac{1}{2}}LU,$$
$$\beta_1=\frac{m_f}{m_f+m_{c_1}},\quad \beta_2=\frac{m_2I_1}{(m_f+m_{c_1})I_2},\quad \beta_3=\frac{m_3I_1}{(m_f+m_{c_1})I_3},$$
$$\bar{c}_{12}=\frac{c_{12}L^4}{EI_1},\quad \bar{c}_{13}=\frac{c_{13}L^4}{EI_1},\quad \bar{c}_{21}=\frac{c_{21}L^4}{EI_2},\quad \bar{c}_{23}=\frac{c_{23}L^4}{EI_2},\quad \bar{c}_{31}=\frac{c_{31}L^4}{EI_3},\quad \bar{c}_{32}=\frac{c_{32}L^4}{EI_3} \tag{14}$$
$$\psi_1=\frac{\rho_{c_1}I_1}{L^2(m_f+m_{c_1})},\quad \psi_2=\frac{\rho_{c_2}I_2}{L^2(m_{c_2})},\quad \psi_3=\frac{\rho_{c_3}I_3}{L^2(m_{c_3})},\quad \lambda_m=\frac{l_m}{L},\quad \lambda_s=\frac{l_s}{L}$$

where L is the CNT length. Using Eq. (14) the dimensionless equations of motion can be expressed as

$$\begin{aligned}
&\frac{\partial^4\eta_1}{\partial\xi^4}-\lambda_s^2\frac{\partial^6\eta_1}{\partial\xi^6}+\frac{\partial^2\eta_1}{\partial\tau^2}+(VCF)^2u_n^2\frac{\partial^2\eta_1}{\partial\xi^2}+2\sqrt{\beta_1}(VCF)u_n\frac{\partial^2\eta_1}{\partial\tau\partial\xi}+\psi_1\lambda_m^2\frac{\partial^6\eta_1}{\partial\tau^2\partial\xi^4}\\
&\qquad-\bar{c}_{12}(\eta_1-\eta_2)-\bar{c}_{13}(\eta_1-\eta_3)=0\\
&\frac{\partial^4\eta_2}{\partial\xi^4}-\lambda_s^2\frac{\partial^6\eta_2}{\partial\xi^6}+\beta_2\frac{\partial^2\eta_2}{\partial\tau^2}+\psi_2\lambda_m^2\frac{\partial^6\eta_2}{\partial\tau^2\partial\xi^4}-\bar{c}_{21}(\eta_2-\eta_1)-\bar{c}_{23}(\eta_2-\eta_3)=0\\
&\frac{\partial^4\eta_3}{\partial\xi^4}-\lambda_s^2\frac{\partial^6\eta_3}{\partial\xi^6}+\beta_3\frac{\partial^2\eta_3}{\partial\tau^2}+\psi_3\lambda_m^2\frac{\partial^6\eta_3}{\partial\tau^2\partial\xi^4}-\bar{c}_{31}(\eta_3-\eta_1)-\bar{c}_{32}(\eta_3-\eta_2)=0
\end{aligned} \tag{15}$$

5. Approximate solution and discretization

To solve Eqs. (15), the Galerkin's approximate method is used. The solution of the dimensionless differential equations are approximated as

$$\eta_1(\xi,\tau)\cong\sum_{r=1}^{N}q_r(\tau)\phi_r(\xi),\qquad \eta_2(\xi,\tau)\cong\sum_{r=1}^{N}q_{r+N}(\tau)\phi_r(\xi),\qquad \eta_3(\xi,\tau)\cong\sum_{r=1}^{N}q_{r+2N}(\tau)\phi_r(\xi) \tag{16}$$

where $q_r(\tau)$, $q_{r+N}(\tau)$ and $q_{r+2N}(\tau)$ are the generalized coordinate of the discretized innermost tube conveying fluid, middle and outermost tubes respectively, and $\phi_r(\xi)$ are the dimensionless eigen-functions of the CNTs that should satisfy the essential and natural boundary conditions. In this work, the boundary conditions are considered as simply supported ends or pinned-pinned which can be written as,

$$\eta=0\quad\text{and}\quad\frac{\partial^2\eta}{\partial\xi^2}=0\qquad\text{at}\quad\xi=0,1 \tag{17}$$

For this boundary condition, considering simple harmonic motion, the comparison functions and generalized coordinate are considered as,

$$\phi_r(\xi)=\sin(r\pi\xi) \tag{18}$$

$$q_r(\tau) = A_r \exp(s_r \tau) \tag{19}$$

where A_r are the dimensionless constant amplitude of the rth-generalized coordinate and s_r denotes the rth mode complex-valued Eigen-frequency.

To discretize equation of motion by Galerkin weighted-residual technique, for the first mode, the wave number is set to 1 and the residual is obtained by substituting Eqs. (16) - (19) into Eq. (15). In this approximate method, the main governing differential equations of motion are used to compute the residue. For this purpose, one generalized coordinate is chosen. In the dimensionless equations (15), the approximate function $\eta(\xi,\tau)$ is substituted by $\sin(\pi\xi)\times q_1(\tau)$ to calculate the residual. Then, this residual is multiplied by a weighting function (test function). Herein, the comparison and weighting functions are the same and are selected as the first mode Eigen-function ($\sin(\pi\xi)$). The resulting weighted residual is then integrated over the domain of the structure and then it is set to zero. This means that the error in the subspace spanned by the trial functions is nullified and only the residual error orthogonal to this subspace would remain. This residual could have components in the complementary subspace of the exact solution not spanned by the information subspace. The trial eigen-functions play the role of the basis functions that span the complementary space of infinite-dimensional space spanning the exact solution. For example, the resulting discretized equation for the innermost tube conveying fluid is obtained as follows

$$\frac{1}{2}\left(\pi^4 + \lambda_s^2\pi^6 - (VCF)^2 u_n^2 \pi^2\right) q_1(\tau) + \frac{1}{2}\left(\psi_1 \lambda_m^2 \pi^4 + 1\right)\ddot{q}_1(\tau) = 0 \tag{20}$$

The coefficient of $q_1(\tau)$ denotes the sum of elastic and geometric stiffness parameters and the coefficient of $\ddot{q}_1(\tau)$ represents the equivalent mass parameter. This process is continued for the next modes; for example, to study the two first modes, the approximate function is considered as $\sin(\pi\xi)q_1(\tau) + \sin(2\pi\xi)q_2(\tau)$.

6. Results and discussion

The material and geometric properties of the CNT and the fluid are shown in Table 1. Results are extracted from the dimensionless parameters and using a MATLAB code. Water is considered as the fluid passing through the CNT. The effects of the aspect ratio, Knudsen number and characteristic lengths on the critical flow velocities are studied.

Table 1. Material and geometric properties of CNT and fluid [10]

Young's modulus (E)	1 Tpa	Fluid viscosity (μ)	1.12×10^{-3} Pa.s
CNT mass density(ρ_c)	2.3×10^{3} kgm^{-1}	Fluid mass density(ρ_f)	1×10^{3}kgm^{-1}
Geometric parameters	$R_1 = 11.9\ nm$ $R_2 = 12.24\ nm$	$R_3 = 12.58\ nm$	$h = 0.34\ nm$
van der Waals parameters	$\varepsilon = 2.968$ meV	$\sigma = 3.407$ Å	$a = 1.42$ Å

In Table 1, the parameters R_1, R_2 and R_3 are the internal radii of the inner, middle and outer CNTs respectively. These parameters are shown in Fig. 1.

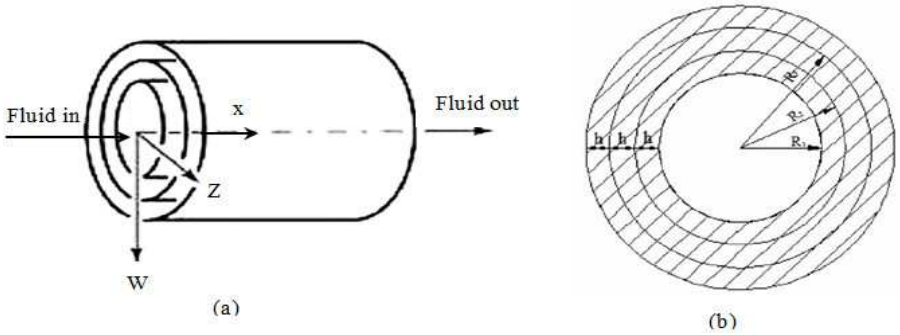

Fig. 1. (a) A fluid conveying TWCNT. (b) Cross sectional view of a circular TWCNT

6.1. Effects of aspect ratio

In this subsection, the effects of aspect ratio on the critical flow velocity and the vibration behavior of CNTs conveying fluid flow are studied using size dependent continuum theory. The critical velocity is a velocity in which the imaginary part of Eigen frequency (natural frequency) reaches zero while its real part (damping) is non-zero and therefore the system is instable. According to Paidoussis [15], by equating the equivalent stiffness of a system (K_{eq}) to zero, the critical value of fluid flow velocity will be obtained. In this case, the divergence instability occurs in the system. Fig. 2 shows the variation of dimensionless critical flow velocity against CNT thickness for the four aspect ratio values of 1, 2, 5 and 10. It can be seen that by increasing the CNT thickness the critical flow velocity decreases. Moreover, the effect of aspect ratio on the critical flow velocity increases as the CNT thickness decreases. Fig. 3 illustrates the imaginary parts of dimensionless fundamental Eigen-frequencies for the nanotube versus dimensionless

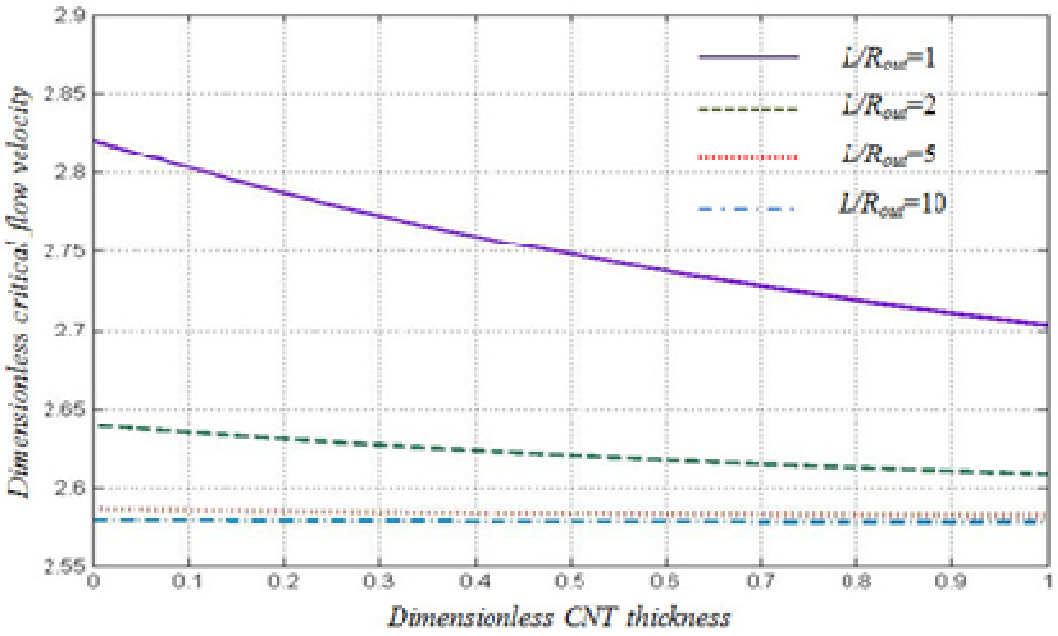

Fig. 2. Dimensionless critical flow velocity against dimensionless CNT thickness for different aspect ratios

flow velocity for the aspect ratio values of 1 and 2, and the dimensionless length scale values of 0.0355 and 0.1. According to Askes and Aifantis [12], for the length scales l_m and l_s large ranges are possible; $l_m = 10 l_s$ is used here for CNT (20, 20). It can be observed that for a certain aspect ratio, the critical flow velocity increases as the characteristic length decreases. For example, by using Table.1, for aspect ratios equal to 1 and 2, approximately 2.30% and 0.58% reductions occur in the magnitude of the critical flow velocities respectively. It means that the divergence instability occurs at a lower critical flow velocity.

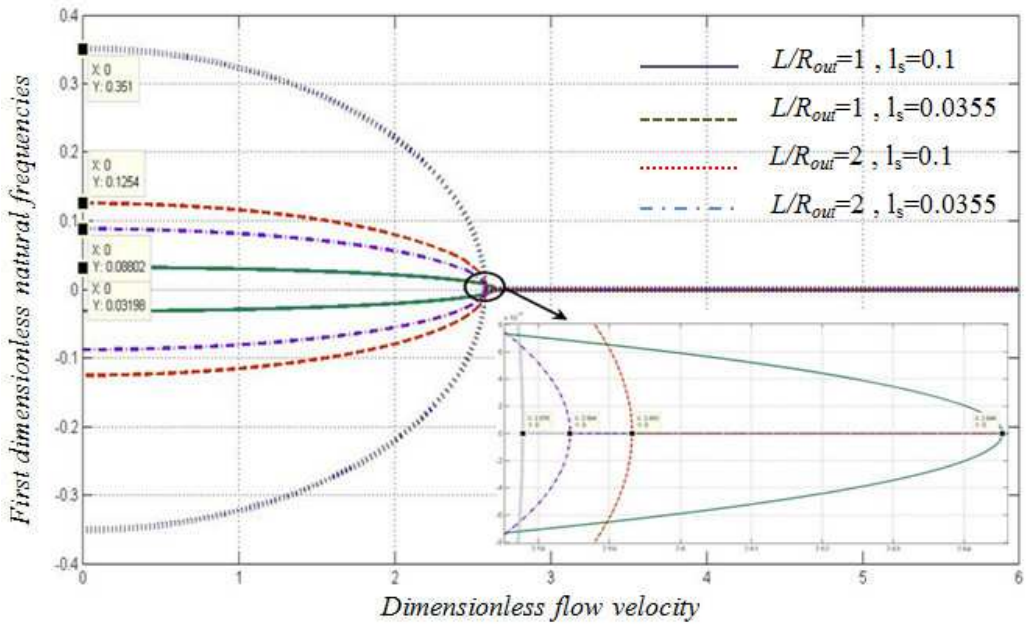

Fig. 3. First dimensionless natural frequency against dimensionless flow velocity for different aspect ratios and characteristic lengths

6.2. Effect of Kn of nano flow

The first and second dimensionless natural frequencies against dimensionless flow velocity for three values of *Kn* are shown in Fig. 4 and 5 respectively. By comparing the values of the critical flow velocities for *Kn* equal to 0, 0.001 and 0.01, the divergence and coupled mode flutter phenomena occur at a lower critical flow velocity as Knudsen number increases. As shown in Figs. 4 and 5, approximately 4.2% and 17.1% reductions occur for increasing the Knudsen number from 0 to 0.001 and from 0.001 to 0.01 respectively. Moreover, as the flow velocity increases, the effect of small-size of nano flow on the natural frequencies increases.

In order to validate the numerical results, the results of Paidoussis [15] are considered. Since Paidoussis investigated the plug flow theory, the Knudsen number is set equal to zero or VCF is substituted by one in Eq. (15). From Figs. 4 and 5 it can be observed that by increasing the flow velocity from zero to its critical value, the natural frequencies approach to zero; as a result, the system's stiffness disappears and divergence mode occurs. As shown in Fig. 4 the first mode divergence is equal to π which is expected from the Paidoussis observations [15].

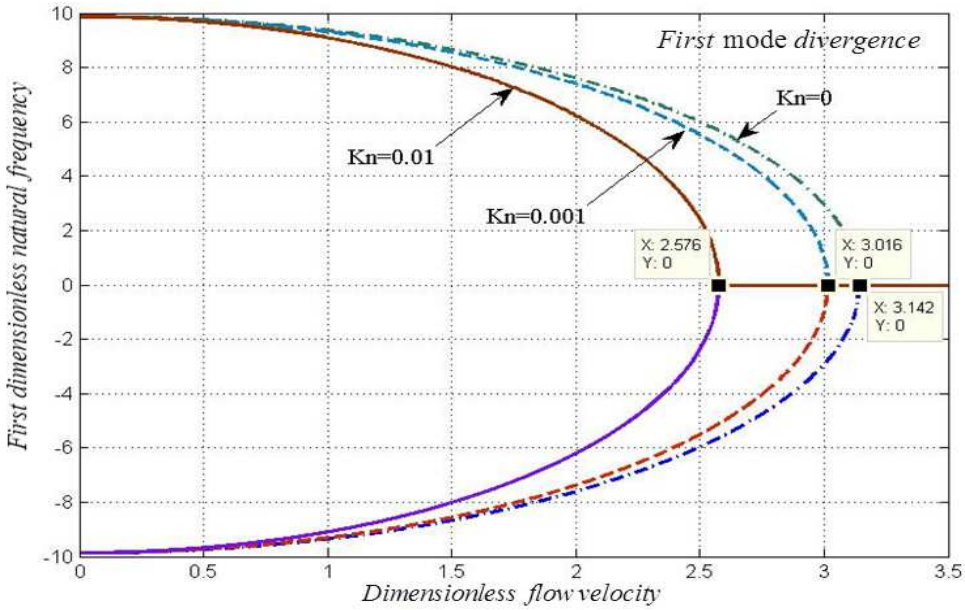

Fig 4. First dimensionless natural frequency versus flow velocity for three values of Knudsen number (Kn=0, 0.001 and 0.01)

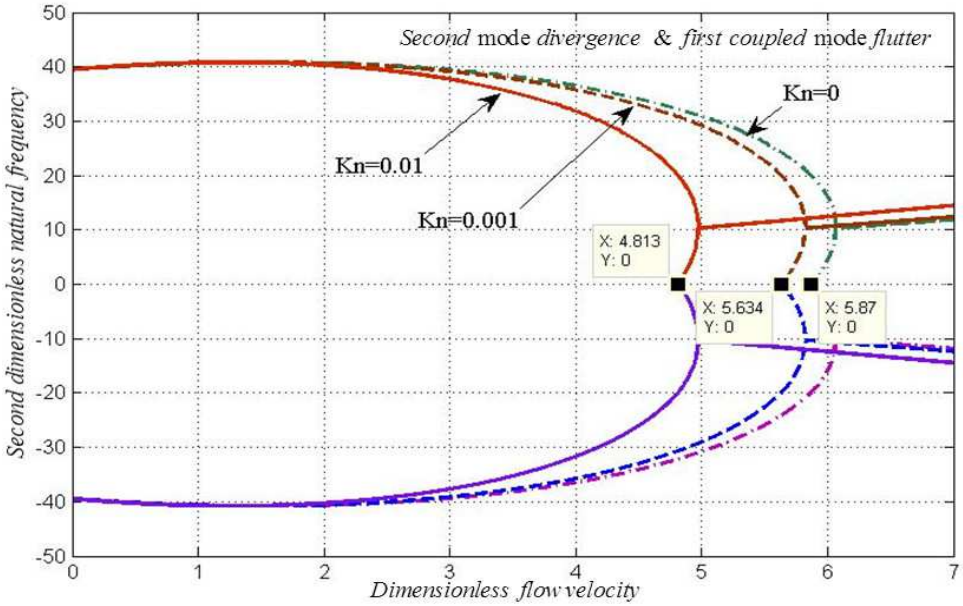

Fig 5. Second dimensionless natural frequency versus flow velocity for three values of Knudsen number (Kn=0, 0.001 and 0.01)

6.3. Simulations of the divergence and flutter instabilities

Fig. 6 shows the variations of the dimensionless natural frequencies versus the dimensionless flow velocities for the first three modes. The Knudsen number is set to be 0.01 and the characteristic length related to the strain gradient is equal to 0.0355. Also, the aspect ratio is considered to be L/Rout=1000. It should be noted that the van der Waals force is the coefficient

of the W term in Eqs. (9) and (10). Hence, by adding these forces, it is expected that the equivalent stiffness be increased. By setting this stiffness term equal to zero, it can be seen that the critical flow velocity value increases. It means that considering the van der Waals force makes the system more stable. Moreover, the dimensionless natural frequencies of three modes decrease as the dimensionless flow velocity increases. By increasing the flow velocity, the first natural frequency reaches to zero at the critical flow velocity value of 2.576 and the system becomes unstable, known as the first divergence instability. Next, by increasing the flow velocity to 4.813, the system becomes stable again. At this point, the frequencies of the first and second modes are coupled which is called the flutter instability. The same phenomenon is occurred at the critical flow velocity equal to 7.219 in which the third divergence and second flutter instabilities occur.

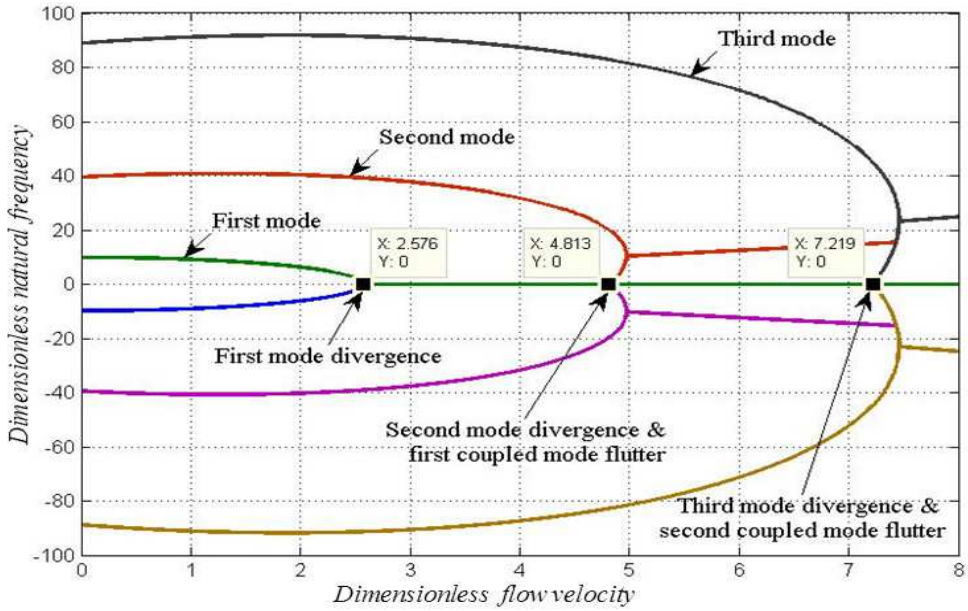

Fig 6. Dimensionless flow velocity dependence of the lowest three modes of a TWCNT

7. Conclusions

The free vibration and instabilities of TWCNT conveying fluid flow were investigated considering the small-size effects of both fluid flow and the structure by using strain-inertia gradient theory. To study the vibration response, the Euler- Bernoulli beam model is used and to calculate the governing equation of fluid-structure interaction, the Galerkin weighted residual method is employed. The variations of the dimensionless critical flow velocities and dimensionless frequencies for different aspect ratios and characteristic lengths in the mentioned theory were examined. It is shown that the flow inside CNTs decreases the system natural frequencies. It means that the fluid flow can destabilize the fluid-structure system. Also it is shown that by increasing the Knudsen number of the passing nano flow, instability occurs at a lower flow velocity value. The results indicate that the critical flow velocity increases as the thickness or outer radius of CNT decreases and it decreases as the CNT length increases.

References

[1] G. Hummer, J.C. Rasaiah, J.P. Noworyta, Water conduction through the hydrophobic channel of a carbon nanotube, Nature, 414 (2001) 188-190.
[2] D. Mattia, Y. Gogotsi, Review: static and dynamic behavior of liquids inside carbon nanotubes, Microfluid Nanofluid, 5 (2008) 289-305.
[3] C.N.R. Rao, A.K. Cheetham, Science and technology of nanomaterials: current status and future prospects, Journal of Materials Chemistry, 11 (2001) 2887-2894.
[4] K. Dong, B.Y. Liu, X. Wang, Wave propagation in fluid-filled multi-walled carbon nanotubes embedded in elastic matrix, Computational Materials Science, 42 (2008) 139-148.
[5] W.J. Chang, H.L. Lee, Free vibration of a single-walled carbon nanotube containing a fluid flow using the Timoshenko beam model, Physics Letters A, 373 (2009) 982-985.
[6] Y. Yan, W.Q. Wang, J.M. Zhang, L.X. Zhang, Free vibration of the water-filled single-walled carbon nanotubes, Procedia Engineering, 31 (2012) 647-653.
[7] M. Rafiei, S.R. Mohebpour, F. Daneshmand, Small-scale effect on the vibration of non-uniform carbon nanotubes conveying fluid and embedded in viscoelastic medium, Physica E: Low-dimensional Systems and Nanostructures, 44 (2012) 1372-1379.
[8] L. Wang, Vibration analysis of fluid-conveying nanotubes with consideration of surface effects, Physica E: Low-dimensional Systems and Nanostructures, 43 (2010) 437-439.
[9] J. Yoon, C.Q. Ru, A. Mioduchowski, Sound wave propagation in multiwall carbon nanotubes, Journal of Applied Physics, 93 (2003) 4801-4806.
[10] Y. Yan, W.Q. Wang, L.X. Zhang, Dynamical behaviors of fluid-conveyed multi-walled carbon nanotubes, Applied Mathematical Modelling, 33 (2009) 1430-1440.
[11] V. Rashidi, H.R. Mirdamadi, E. Shirani, A novel model for vibrations of nanotubes conveying nanoflow, Computational Materials Science, 51 (2012) 347-352.
[12] H. Askes, E.C. Aifantis, Gradient elasticity and flexural wave dispersion in carbon nanotubes, Physical Review B, 80 (2009) 195412.
[13] M. Mirramezani, H.R. Mirdamadi, M. Ghayour, Innovative coupled fluid–structure interaction model for carbon nano-tubes conveying fluid by considering the size effects of nano-flow and nano-structure, Computational Materials Science, 77 (2013) 161-171.
[14] W.G. Polard, R.D. Present, On gaseous self-diffusion in long capillary tubes, Physical Review, 73 (1948) 762.
[15] M.P. Paidoussis, Fluid-structure interactions: slender structures and axial flow, Academic press, 1998.